Chapter 11
Greedy Source Placement Optimization for MIMO Control of Ground-Based Vibration Tests

Chandler Smith, Timothy Walsh, Wilkins Aquino, Drew Kouri, and Ryan Schultz

Abstract In this work, we investigate the effectiveness of greedy algorithms in optimizing the placement of electrodynamic shakers to achieve optimal control in Multiple-Input Multiple-Output (MIMO) vibration tests. In the context of ground-based vibration tests, control algorithms are used to estimate excitation signals that will produce a specific vibration response in the test object. The challenges in control lie in estimating the drive signal, which is inherently an inverse problem, and in satisfying the limited input energy available from the shaker's power. To this end, we investigate an inverse problem formulation that allows the user to weight their preference for matching target response data versus minimizing the demand on input power. The success of the proposed algorithm depends critically on the shaker locations, where poor placement results in diminished controllability resulting in unachievable drive powers and(or) lack of proper control of the system.

Optimizing the placement of sources is a Mixed Integer Programming (MIP) optimization problem, known for its computational expense and complexity. Greedy algorithms present a potential solution by trading optimality for enhanced computational performance. In our research, we conduct a comparative analysis between a greedy algorithm and Gurobi, a powerful optimization tool for solving MIP problems, to evaluate the greedy algorithm's capability in identifying effective shaker locations.

Our results demonstrate that the greedy algorithm often matches solutions to the MIP program. In addition, our study indicates that the ideal placement of the shakers is influenced by the user's preference for minimizing input energy versus achieving target response accuracy. This highlights the importance of customizable parameters in achieving optimal system control through strategic source placement.

Introduction

Ground-based vibration testing using Multiple Input Multiple Output (MIMO) control is an advanced technique for simulating flight environments in order to evaluate the dynamic behavior of the vehicle and its components. MIMO control involves the simultaneous application of multiple excitation forces and the measurement of responses at multiple points. This approach provides a more comprehensive understanding of the structural dynamics, enabling the accurate reconstruction of the system's dynamic response during operation in a flight environment. However, MIMO control also presents many challenges, which can significantly impact the effectiveness and accuracy of the vibration testing. This work focuses on two of those challenges: the spatial configuration of the electrodynamic shakers (sources) and the control strategy.

There are a few key considerations when placing sources and choosing a control strategy used to determine the excitation signals of the driving shakers. First, the control strategy and placement of the shakers must be carefully chosen to effectively excite the expected dynamic response produced in a flight environment. For example, authors in [1] demonstrated how the quality of a shock response MIMO test changes with actuator locations. Second, the shakers must be placed in physically feasible locations given the constraints of the testing space and test article. Third, the shakers maximum force capacity and

Chandler Smith · Timothy Walsh · Drew Kouri · Ryan Schultz
Sandia National Laboratories, Albuquerque, NM 87185
e-mail: chasmit@sandia.gov; tfwalsh@sandia.gov; dpkouri@sandia.gov; rschult@sandia.gov

Wilkins Aquino
Department of Civil and Environmental Engineering, Duke University, Durham, N.C.
e-mail: waquino@sandia.go

Matthew Allen et al. (eds.), *Special Topics in Structural Dynamics & Experimental Techniques, Vol. 5*, Conference Proceedings of the Society for Experimental Mechanics Series, https://doi.org/10.13052/97887-438-0150-4_11

output energy are finite; hence shaker configurations and control strategies should ensure that the available energy is evenly distributed across all the shakers [2]. A general framework for approaching the optimal source placement problem is as follows: i) select a control strategy, ii) determine a quantitative measure of the quality of the source configuration, and iii) optimize the source locations by maximizing the selected metric.

In the context of structural dynamics, optimal control and source placement applications has largely focused in the area of active structural damping for mitigating vibrations [3]. Conceptually, MIMO control and active damping are similar in that the goal is to achieve a desired structural state with minimal energy. Much of this theory is based on state-space formulations with a critical focus on placing source that maximize controllability [4]. Research on source placement for MIMO vibration testing is less prolific in the literature. In [5], a greedy-based approach was taken to select actuators that minimized the output energy of the actuator in order to achieve a desired random vibration specification. In [6], another greedy search method was proposed, which aimed to minimize the random vibration frequency response match to some target response. This method performed well compared to a brute force exhaustive search.

Regardless of the method, source placement optimization involves solving an NP-hard mixed integer optimization problem. While branch and bound methods can be employed, they are significantly constrained by problem size due to their computational complexity. As a more efficient alternative, greedy optimization approaches can be used, offering faster solutions at the expense of optimality. Greedy search algorithms involve iteratively adding sensors one at a time, each time choosing the sensor that minimizes some user-specified objective function.

In this work, we develop a MIMO control and source placement optimization framework. The core of the approach involves solving a regularized inverse problem, which ensures stability and robustness in the presence of measurement errors, while providing a user-specified regularization parameter that controls the trade-off between the fidelity to the target dynamic response and the smoothness and magnitude of the control inputs.

We propose two source placement optimization strategies that use a greedy search algorithm and compare these designs by applying them to the regularized inverse problem control strategy. The first method seeks to directly minimize the objective function corresponding to the l_2-norm regularized inverse problem, with the solution depending on the user-selected regularization parameter. Recognizing that the greedy search is not guaranteed to provide a near-optimal or optimal solution, we compare this method to an equivalent mixed-integer quadratic programming (MIQP) problem and to randomized brute force search.

Inspired by the optimal sensor placement literature, the second proposed source optimal experiment design (OED) framework aims to minimize the E-criterion. The E-criterion benefits from guarantees on the quality of the greedy-generated solution [7], and has the added advantage of being independent of the choice of regularization parameter and of the target response data. In this work, we show that minimizing the E-criterion also indirectly minimizes the input energy of the least squares control solution.

We compare the two source placement OED frameworks in terms of their performance in solving the l_2-norm regularized inverse problem. The control and source placement framework is applied to a MIMO problem that seeks to reproduce the dynamic response of a sharp cone flight vehicle subjected to a turbulence-induced, fluctuating pressure field using a limited number of shakers.

This work is broken down into the following sections. The Background and Methodology section describes the MIMO control formulation followed by the proposed source placement optimization algorithms. In the MIQP Greedy Search Comparison section, we compare the performance of the l_2-norm regularized greedy search method to the MIQP problem in terms of solution accuracy and computational runtime. In the Greedy OED Performance on Full-Scale Model section, we investigate the performance of the greedy method on a full-scale wind tunnel model. In this section, we also compare the E-optimal design and l_2-norm regularized designs, and investigate their robustness to changes in the regularization parameter used to solve the control inverse problem.

Background and Methodology

Assume we are given a target response $\hat{u}_o(\omega)$ where ω is angular frequency and a maximum number of actuators N. The goal is to find sources $s(\omega) \in \mathbb{C}^d$, with $d \leq N$, and their locations such that the output response $u(\omega)$ of the MIMO vibration test is close to $\hat{u}_o(\omega)$.

Assuming the structural response is defined by a Linear Time Invariant system, the map from the sources to the acceleration is taken as

$$u(\omega) = H(\omega)s(\omega), \tag{1}$$

where $H(\omega) : \mathbb{C}^d \to \mathbb{C}^n$ is the transfer operator (or system frequency response function matrix), $u(\omega) \in \mathbb{C}^n$ is the acceleration response, and $s(\omega) \in \mathbb{C}^d$ is the source vector.

To solve this inverse problem, we introduce an l_2-norm regularization term to form the Tikhonov regularization problem. The regularized control inverse problem is taken as,

$$\min_{s(\omega)\in\mathbb{C}^d} \frac{1}{2}\left\|H(\omega)s(\omega)-\hat{u}_o(\omega)\right\|^2+\frac{\lambda}{2}\left\|s(\omega)\right\|^2, \tag{2}$$

where $\lambda > 0$ is the regularization parameter that controls the trade-off between the fidelity to the target response and the smoothness of the solution. The l_2-norm regularization can be interpreted as a way of minimizing the total energy in the solution. In this context, the energy of the control inputs s is quantified by

$$\frac{1}{N_\omega}\sum_{i=1}^{N_\omega}||s(\omega_i)||^2=\frac{1}{N_\omega}\sum_{i=1}^{N_\omega}\sum_{k=1}^{d}s_k(\omega_i)^2 \tag{3}$$

where N_ω represents the total number of frequency lines. By including the regularization term, $\lambda||s||^2$, we penalize large values of s, which in turn, encourages solutions with smaller magnitudes. This may be useful in practical applications where excessive energy may be undesirable.

The optimization problem in equation 2 can be solved analytically for each frequency line with the following closed-form solution:

$$s^*(\omega)=\left(H(\omega)^TH(\omega)+\lambda\mathbb{I}\right)^{-1}H(\omega)^T\hat{u}_o(\omega). \tag{4}$$

In this work, the regularization parameter is assumed constant across all frequencies.

Now that a control strategy is defined, we propose a source placement optimization algorithm. Consider a candidate index set $\mathscr{I} := \{1,\ldots,d\}$ that corresponds to all d possible source (actuator) locations. The goal of source placement optimization to find, at most, N sources that minimizes equation 2.

To this end, we propose the following Mixed Integer Quadratic Programming (MIQP) problem:

$$\begin{aligned}\theta^*,z^*(\omega)=\min_{x,\theta,z}\quad & \frac{1}{2N_\omega}\sum_{j=1}^{N_\omega}\left(\left\|H(\omega_j)z(\omega_j)-\hat{u}_o(\omega_j)\right\|^2+\lambda\left\|z(\omega_j)\right\|^2\right)\\ \text{s.t. } & \theta_is_i(\omega)=z_i(\omega)\quad \text{for } i\in\mathscr{I}\\ & \theta_i\in\{0,1\}\\ & \sum_{i=1}^{d}\theta_i\le N,\end{aligned} \tag{5}$$

where θ_i is a boolean, s_i and z_i indicate the i^{th} entry of $s(\omega)$ and $z(\omega)$ respectively, and $z(\omega)\in\mathbb{C}^d$ is defined by the equality constraint.

MIQP problems are difficult to solve and computationally expensive. Hence, we propose a greedy search algorithm, which significantly reduces computational cost but at the expense of solution optimality. In the greedy search, let $\theta\in\mathscr{P}=\{i_1,\ldots,i_N\}\subset\mathscr{I}$ represent the selected source indices, and let $s^*(\omega,\theta)$ and $H(\omega,\theta)$ represent the solution to the control problem and map, respectively, corresponding to the source locations indexed in θ. The greedy algorithm seeks to minimize the function $f(\theta)$, which is given by

$$f(\theta)=\frac{1}{2}\sum_{\omega}\left(\left\|H(\omega,\theta)s^*(\omega,\theta)-\hat{u}_o(\omega)\right\|^2+\lambda\left\|s^*(\omega,\theta)\right\|^2\right), \tag{6}$$

where $s^*(\omega,\theta)$ is the optimal control input given by equation 4 evaluated at the source locations θ. As described in Algorithm 1, we first initialize an empty set θ, then search over all candidate source locations, selecting the best source location that minimizes $f(\theta)$, and adding it to the set θ. The process is repeated until the source budget is satisfied.

In addition to the Tikhonov regularization objective function, we consider the greedy algorithm using the E-criterion. In this context, the E-criterion is taken as

$$f(\theta):=\frac{1}{N_\omega}\sum_{j=1}^{N_\omega}\sigma_{max}\left(H(\omega_j,\theta)^TH(\omega_j,\theta)\right)^{-1}. \tag{7}$$

where σ_{max} is the largest singular value of $\left(H(\omega,\theta)^TH(\omega,\theta)\right)^{-1}$. Typically, E-optimality is defined by the maximum eigenvalue [7], however, we will use the singular values since H^TH is positive semi-definite, and hence the eigenvalues and singular values are equivalent.

Algorithm 1 Greedy Algorithm

1: $s^*(\omega,\theta) = \left(H(\omega,\theta)^T H(\omega,\theta) + \lambda \mathbb{I}\right)^{-1} H(\omega,\theta)^T \hat{u}_o(\omega)$
2: $f(\theta) = \frac{1}{2N_\omega}\sum_{j=1}^{N_\omega}\left(\left\|H(\omega_j,\theta)s^*(\omega_j,\theta) - \hat{u}_o(\omega_j)\right\|^2 + \lambda\left\|s^*(\omega_j,\theta)\right\|^2\right)$
3: **Initialization**: $\theta = \emptyset$ and $M = 0$
4: **while** $M < N$ **do**
5: $\quad \theta_j = \theta \cup \{j\}$
6: $\quad j^* = \underset{j\in\{1,\ldots,n\}\setminus S}{\arg\min}\ f(\theta_j)$
7: $\quad \theta = \theta \cup \{j^*\}, \quad M = M+1$
8: **end while**

The E-criterion is motivated by several considerations. The E-optimal design maximizes the minimum eigenvalue of $H^T H$. This can be interpreted as maximizing information by ensuring a more uniform distribution of information across all measurement directions. Additionally, maximizing the minimum eigenvalue tends to minimize the matrix condition number, which leads to more stable and reliable solutions to the inverse problem. The use of the E-criterion may also be more practical in some settings since it does not require the target response.

We also expect that E-optimal designs minimize the input energy of the least squares solution, since $\sigma_{max}\left(H^T H\right)^{-1}$ contributes to an upper bound on the input energy. This follows directly from the definition of the least squares squares solution (i.e. $\lambda = 0$) and the norm inequality,

$$
\begin{aligned}
\hat{x}_{lsq} &= (H^T H)^{-1} H^T \hat{u}_o, \\
||\hat{x}_{lsq}||_2 &= \left\|(H^T H)^{-1} H^T \hat{u}_o\right\|, \\
&\leq \left\|(H^T H)^{-1} H^T\right\| \|\hat{u}_o\|, \\
&= \sigma_{max}\left((H^T H)^{-1} H^T\right) \|\hat{u}_o\| \\
.
\end{aligned} \tag{8}
$$

where the matrix norm is taken as the spectral norm, i.e. the maximum singular value of the matrix. Finally, we observe that minimizing $\sigma_{max}\left((H^T H)^{-1} H^T\right)$ is equivalent to minimizing the E-criterion by the definition of the singular value decomposition:

$$
\begin{aligned}
\sigma_{max}\left((H^T H)^{-1} H^T\right) &= 1/\sigma_{max}(H), \\
&= \sqrt{\sigma_{max}\left(H^T H\right)^{-1}}.
\end{aligned} \tag{9}
$$

The final motivation for E-optimality is that the criterion is approximately supermodular [7]. Supermodularity guarantees that the greedy algorithm results in a near-optimal solution. The proof of approximate supermodularity is based on sensor placement optimization [7]. However, we can show that these results are applicable to the source placement problem by leveraging the fact that non-zero singular values of H and H^T are equivalent. We leave this derivation for future work.

Example Problem

In this work, we use a simulation of a wind tunnel test article subjected to turbulence to verify and demonstrate the proposed methods. The goal of this work is to optimally place a small set of virtual actuators to best reproduce the dynamic response generated from a wind tunnel environment.

The wind tunnel serves to reproduce turbulence-induced, fluctuating pressure loads experienced by a flight vehicle. To this end, the turbulent boundary layer and surface quantities were simulated using Sierra-SPARC's hypersonic computational fluid dynamics (CFD) code [8], and converted to a discretized pressure cross power spectral density (CPSD) on the surface of the sharp cone FEM using an extension to the Corco's model [9]. Time-domain pressures were realized from the pressure CPSD and then Fourier transformed into the frequency domain to obtain the problem form given in equation 1. The frequency domain acceleration response due to the fluctuating surface pressure was simulated using the structural FEM simulation code Sierra-SD [10]. The target acceleration responses are measured in the y and z degrees of freedom at 84 nodes as shown in Figure 1. The discretized pressure patches on the model's surface also serve as the candidate shaker (source) locations, totaling 782 locations. Given the CFD turbulence model and the frequency range of interest, most of the pressure loading was towards the aft end of the vehicle.

The frequency range of interest was from one to three kHz. The vehicle deformation was dominated by four modes: two first order bending modes, and two second order bending modes. The first and second order bending modes are shown in Figure 2.

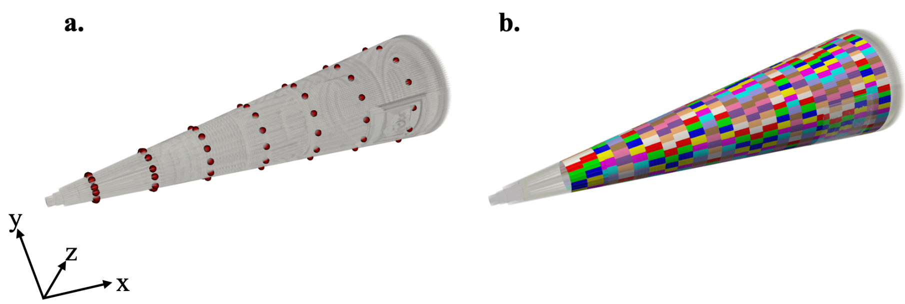

Fig. 1 a) The target response locations and b) the candidate source locations.

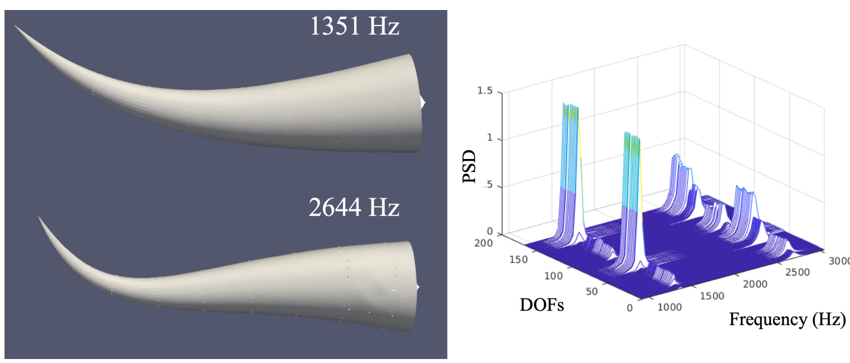

Fig. 2 Power spectral density and major resonances of structural FEM.

MIQP Greedy Search Comparison

In this section, we evaluate the quality of the greedy source placement algorithm's solution by comparing it to the optimal solution to the MIQP problem, solved using Gurobi's MIQP solver [11]. This method serves as a form of verification for the Greedy algorithm using the regularized inverse problem objective function. Gurobi uses a branch and bound technique to solve the MIQP problem [11]. For this initial study, we simplified the problem to ensure the MIQP problem could be solved in a reasonable amount of time. Specifically, the OED algorithms included only one frequency line corresponding to the first bending mode of the structural model. The map H is complex-valued with 168 rows and 100 columns, representing a small subset of all possible source locations. We set $\lambda = 10^{-3}$ in order to provide numerical stability to Gurobi's optimization algorithm. When solving the regularized inverse problem, $\lambda = 10^{-3}$ resulted in a solution close to the least squares solution.

We first verified the solution to the MIQP by comparing it to 50,000 randomly selected sources. We ran the optimization algorithm for five source budgets (one through five). We then computed the quantile of the MIQP solution with respect to randomly selected sources by counting the number of times that the MIQP solution $f(\theta^*_{mip})$ was less than the random sensor solution $f(\theta^i_{random})$ for $i = 1, \ldots, 50,000$. The quantile is defined as:

$$quantile = \frac{1}{50,000} \sum_{i=1}^{50,000} \mathscr{B}\left(f(\theta^*_{mip}) \leq f(\theta^i_{random})\right),$$

where $\mathscr{B}$ returns one if true and zero if false. Table 1 summarizes the results for the five different budgets. For each source budget, the MIQP solution outperforms 100% of the randomly selected source combinations.

We then performed the same study using the greedy algorithm and computed its quantiles, which are also included in table 1. While the Greedy method performs well, it clearly results in suboptimal solutions, and in some case is outperformed by a brute force random search. For example, the greedy solution outperformed 90% of the randomly selected sources for a source budget of four. However, the differences between the objective $f(\theta)$ using greedy and the MIQP method were relatively small.

Table 1 Quantiles and optimal objective values for MIQP and greedy solutions

Budget	1	2	3	4	5
MIP Objective Value	0.1297	2.090e-3	3.225e-4	2.321e-4	1.517e-4
Greedy Objective Value	0.1297	4.020e-3	6.606e-4	2.825e-4	2.301e-4
MIP Quantile	1.000	1.000	1.000	1.000	1.000
Greedy Quantile	1.000	0.928	0.992	0.898	0.997

We now investigate the accuracy of the greedy search relative to the MIQP problem as a function of the regularization parameter. For this investigation, we solved individual source placement optimization problems for regularization parameters ranging from $\lambda = 10^{-3}$ to $\lambda = 10^{10}$. For each regularization parameter and the corresponding optimal source design, we solved the a control inverse problem using the same regularization parameter. The results of this study are presented as Pareto curves in Figure 3.

The Pareto curve presents the residual, $\|H(\theta^*)s^*(\theta^*) - \hat{u}_o\|^2$, as a function of the input energy, $||s^*(\theta^*)||^2$, where θ^* indicates optimal source design, for all regularization parameters of interest. The Pareto curve helps visualize the trade-off between the residual and the input energy. We emphasize for clarity that a source placement optimization problem was solved for each regularization parameter. Figure 3 indicates that the Greedy and MIQP algorithms exhibit similar performance in terms of the residual and input energy. For some regularization parameters, the Greedy algorithm outperformed the MIQP by a small, negligible amount. We expect this was because the MIQP did not completely converge.

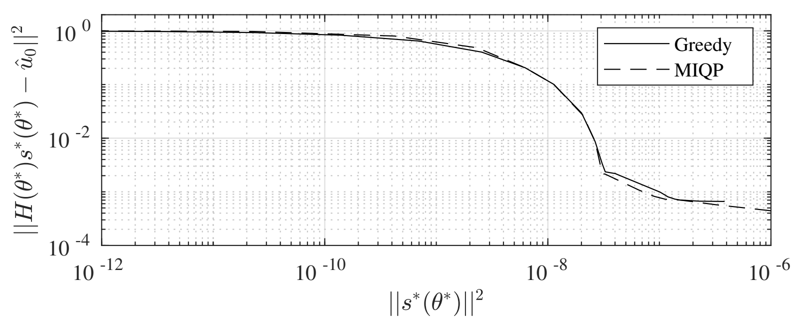

Fig. 3 Pareto curve of solutions using the greedy search algorithm and MIQP for one hundred candidate input locations with a total source budget of three.

One of the drawbacks of attempting to solve the full MIQP OED problem is the extensive runtime. While the greedy method results in suboptimal solutions, it completes in seconds. In contrast, the MIQP can take hours to solve even relatively small problems, and its computational cost increases with the source budget and the total number of candidate source locations.

In this study, we investigated the MIQP runtime as a function of the source budget and the total number of candidate source locations. We ran Gurobi on 16 CPUs with a base clock speed of 2.7 GHz. We generated a single-frequency, strictly real transfer matrix with 168 target response degrees of freedom (DoFs). We varied the source budget from one to five and the total candidate source locations from 100 to 600. Figure 4 presents the runtime in minutes for each budget on a logarithmic scale. The maximum observed runtime was approximately 300 minutes. These performance results by no means represents the optimal performance of Gurobi, only our observation using finite computing resources and the optimizer's default options.

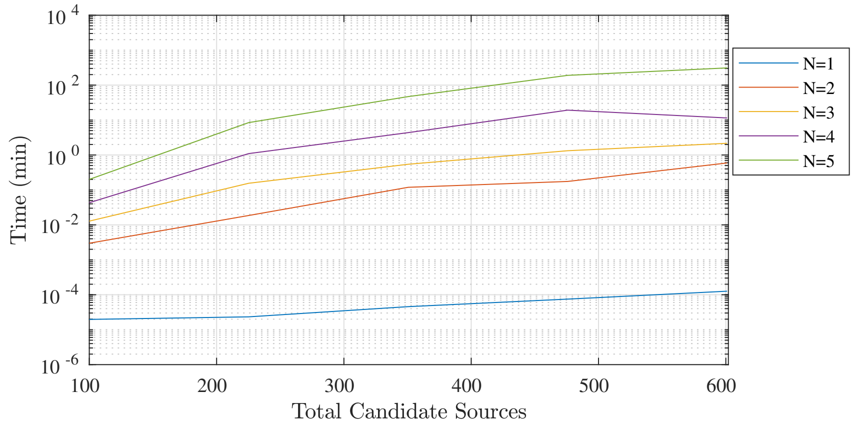

Fig. 4 MIQP solver runtime using Gurobi as a function of total candidate source locations and source budget (N).

Greedy OED Performance on Full-Scale Model

In this section, we applied the greedy source placement algorithms to the full wind tunnel model over a wide band of frequencies. The optimization algorithms include 71 frequency lines spanning one to three kHz. In this example, we set the source budget equal to 5, and include all 168 target response DoFs and all 782 candidate source locations $\left(H(\omega_i) \in \mathbb{C}^{168\times782}\right)$.

We focus on three source configurations using the greedy algorithm corresponding to the following objective funcitons: i) E-optimality, ii) the regularized objective with $\lambda = 1.7\times10^6$, denoted *Tikhonov* $\lambda = 1.7\times10^6$, and iii) the regularized objective with $\lambda = 10^{-3}$, denoted *Least Squares*. Each criterion was chosen because of their unique spatial configurations as shown in Figure 5. The *Least Squares* design (Figure 5a.) favored sources near the aft end of the vehicle as this is where most of the pressure generating the target response occurs. In other words, encouraging minimum residual over minimum input energy resulted in sources physically close to the true source locations. The *Tikhonov* $\lambda = 1.7\times10^6$ design encouraged lower source energy, which resulted in a clustering of sources near the nose of the vehicle (Figure 5b.). The result is intuitive since we expect the largest dynamic response magnification at the nose due to the vehicle's active bending modes. Finally, the E-optimal criterion results in a design that is visually between the two previous scenarios, spreading the sources evenly across the model (Figure 5c.).

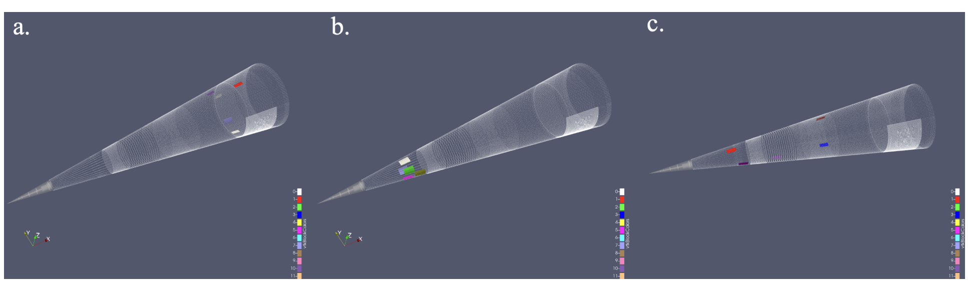

Fig. 5 a) The *Least Squares* OED solution, b) the OED solution using Tikhonov regularization with $\lambda = 1.7\times10^6$, and c) the OED solution using E-optimality.

We first confirmed that the Greedy algorithm resulted in good solutions relative to random source placement. For each of the three optimality criteria, we drew 5,000 unique random combinations of 5 source locations and evaluated the corresponding OED objective function for each sample. Figure 6 presents the histograms of the three objective functions evaluated at the random samples alongside the solution to the OED. In each of the three cases, the greedy search resulted in better solutions than the randomized search.

In the next studies, we investigate the design performance of each of the three solutions by plotting their Pareto curves. To generate a Pareto curve, we used the optimal designs from the three cases: i) *Least Squares*, *Tikhonov* $\lambda = 1.7\times10^6$, and *E-Optimal*, and solved the regularized inverse problem for all values of λ. In these studies, λ ranged from 10^{-3} to 10^{10}. The

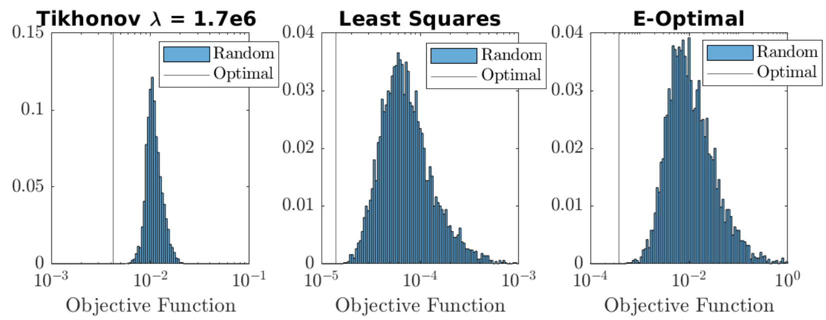

Fig. 6 a) OED solution using least squares formulation. b) OED solution using Tikhonov regularization with $\lambda = 1.7 \times 10^6$. c) OED solution using E-criterion..

Pareto curve then plots the residual, taken as,

$$Residual = \frac{1}{N_\omega} \sum_{i=1}^{N_\omega} ||H(\omega_i)s^*(\omega_i) - \hat{u}_o(\omega_i)||^2,$$

as a function of input energy, taken as,

$$Input\ Energy = \frac{1}{N_\omega} \sum_{i=1}^{N_\omega} ||s^*(\omega_i)||^2.$$

The Pareto curves are shown in Figure 7 along a reference Pareto curve corresponding to the optimal design as a function of λ denoted *Tikhonov All* λ. The reference curve was obtained by solving the l_2-norm regularized source placement problem and the regularized inverse problem with the same value of λ.

One of the take-aways of this work is that the optimal source locations vary with the choice of λ. For instance, the source locations optimized with $\lambda = 10^{-2}$ do not necessarily yield optimal results when the control inverse problem is solved with $\lambda = 10^3$. We observe this behavior by comparing the reference Pareto curve (*Tikhonov All* λ) to the other fixed design cases, and note the improvement in the solution to the inverse problem in terms of fidelity to the target response and input energy when λ is consistent between the inverse problem and the source placement algorithm.

We also use Figure 7 to interpret how robust the optimized source design is to changes in the regularization parameter. For context, there are likely cases in practice that the source configuration is first chosen, but then the regularization parameter used to solve the inverse problem is adjusted to improve the control performance. Inspecting Figure 7, we observe that the *Least Squares* design results in a smaller residual than the E-optimal design and *Tikhonov* $\lambda = 1.7 \times 10^6$. If we are interested in control solutions that both minimize input energy and residual then we would likely prefer the *Tikhonov* $\lambda = 1.7 \times 10^6$ design. However, this design's fidelity to the target response is limited as indicated by the flat curve plateau. Based on the Pareto curve and physical positions on the vehicle, the *E-Optimal* design tends to strike a balance between the two extreme designs.

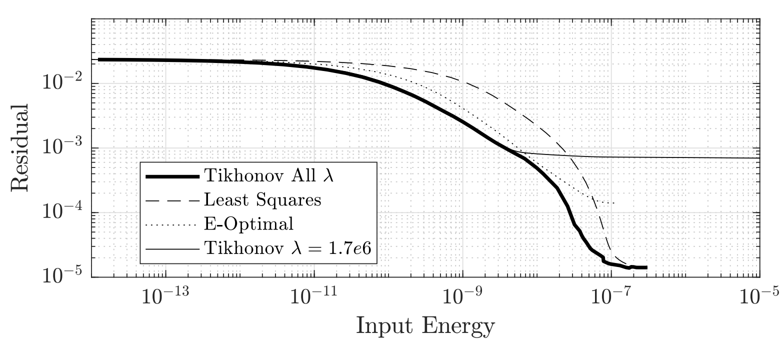

Fig. 7 Pareto curve for three fixed greedy-based designs: *Least Squares* (dashed), *Tikhonov* $\lambda = 1.7 \times 10^6$ (solid), and *E-Optimality* (dotted). *Tikhonov All* λ (thick solid) plots the residual and input energy corresponding to multiple source designs obtained from the regularized objective where each design is optimized for each λ.

Conclusion

We conclude this work with the following observations. The greedy algorithm performs well compared to the MIQP method, but is not hindered by computational runtime. This allowed us to solve larger problems in terms of number of frequency lines, candidate input locations, and total source budget with minimal computational effort. We also demonstrated the advantages in choosing the regularization parameter in the source placement optimization algorithm in a manner consistent with the inverse control problem. Finally, we conclude that each of the designs studied in this chapter had a notable trade-off between the fidelity to the target response and the magnitude of the inputs. From the practitioner point of view, these trade-offs should be investigated prior to assembling the test and weighed according to the total source budget and physical energy constraints of the equipment.

Acknowledgments Sandia National Laboratories is a multi-mission laboratory managed and operated by National Technology & Engineering Solutions of Sandia, LLC (NTESS), a wholly owned subsidiary of Honeywell International Inc., for the U.S. Department of Energy's National Nuclear Security Administration (DOE/NNSA) under contract DE-NA0003525. This written work is authored by an employee of NTESS. The employee, not NTESS, owns the right, title and interest in and to the written work and is responsible for its contents. Any subjective views or opinions that might be expressed in the written work do not necessarily represent the views of the U.S. Government. The publisher acknowledges that the U.S. Government retains a non-exclusive, paid-up, irrevocable, world-wide license to publish or reproduce the published form of this written work or allow others to do so, for U.S. Government purposes. The DOE will provide public access to results of federally sponsored research in accordance with the DOE Public Access Plan.

References

1. Schultz, R. "Explorations in multiple-input shaker shock testing." (2019).
2. Behling, M., Allen, M.S., Mayes, R.L., DeLima, W.J., and Hower, J. "Influence of shaker limitations on the success of mimo environment reconstruction". In *Dynamic Environments Testing, Volume 7*, pages 115–129, Cham (2024). Springer Nature Switzerland.
3. Akhatb, R. and Golnaraghi, M.F. "Active structural vibration control: a review". *The Shock and Vibration Digest*, 35(367) (2003).
4. Georges, D. "The use of observability and controllability gramians or functions for optimal sensor and actuator location in finite-dimensional systems". In *Proceedings of 1995 34th IEEE Conference on Decision and Control*, volume 4, pages 3319–3324 vol.4 (1995).
5. Mayes, R., Ankers, L., Dabor, P., Moulder, T., and P., I. "Optimization of shaker locations for multiple shaker environmental testing". *Experimental Techniques*, 44 (2019).
6. Rohe, D.P., Nelson, G.D., and Schultz, R.A. "Strategies for shaker placement for impedance-matched multi-axis testing". In *Sensors and Instrumentation, Aircraft/Aerospace, Energy Harvesting & Dynamic Environments Testing, Volume 7*, pages 195–212, Cham (2020). Springer International Publishing.
7. Chamon, L. and Ribeiro, A. "Approximate supermodularity bounds for experimental design". *CoRR*, abs/1711.01501 (2017).
8. Howard, M., Bradley, A., Bova, S.W., Overfelt, J., Wagnild, R., Dinzl, D., Hoemmen, M., and Klinvex, A. *Towards Performance Portability in a Compressible CFD Code*. Number 0 in AIAA AVIATION Forum. American Institute of Aeronautics and Astronautics (2017).
9. DeChant, L.J. and Casper, K.M. *Pressure Fluctuation Longitudinal Coherence: An Extended Model*. Number 0 in AIAA SciTech Forum. American Institute of Aeronautics and Astronautics (2021).
10. Bunting, G., Crane, N., Day, D., Dohrmann, C., Ferri, B., Flicek, R., Hardesty, S., Lindsay, P., Miller, S., Munday, L., et al. "Sierra structural dynamics users notes 4.50.". Technical report, Sandia National Lab.(SNL-NM), Albuquerque, NM (United States) (2018).
11. Gurobi Optimization, L. "Gurobi optimizer reference manual" (2024).